STM JOURNALS

Journal of Offshore Structure and Technology

Volume 1, Issue 1
www.stmjournals.com

Vortex Shedding Characteristics of Tapered Cylinders at Turbulent Wake

Vahid Tamimi**, Mostafa Zeinoddini, Arash Bakhtiari
Department of Civil Engineering, K.N.Toosi University of Technology, Tehran, Iran

Abstract

The physics of flow regime around a tapered cylinder is strongly three-dimensional (3D) and complex. These pose numerical difficulties in capturing the vortex shedding phenomena in the wake of cylinder. This paper discusses the main characteristics of vortex shedding behind a fixed linearly tapered circular cylinder at relatively high Reynolds numbers. A computational fluid dynamics model is employed to solve the 3D incompressible transient Navier-Stokes governing equations. The numerical model is first calibrated/validated against available experimental and Direct Numerical Simulations data for vortex shedding past circular cylinders from other researchers. The calibrated model is then employed to explore vortex shedding characteristics behind a stationary and mildly tapered cylinder. A range of Reynolds number up to 29,000 is considered. The model is able, reasonably well, to simulate key physical vortex shedding characteristics for tapered cylinders. Phenomena such as variation of the shedding frequency along the cylinder span or cellular vortex shedding, vortex dislocations or vortex splitting, oblique vortex shedding, streamwise or longitudinal vortices and the variation of the vorticity patterns along the tapered cylinder are discussed. Lift and drag force coefficients of the tapered cylinder are also presented.

Keywords: *Tapered cylinder, cellular and oblique vortex shedding, vortex dislocations, lift and drag forces*

****Author for Correspondence*** Email: vahidtamimi@sina.kntu.ac.ir

INTRODUCTION

Tapered circular cylinders or truncated cones are employed in a variety of engineering applications. Common examples are legs of the gravity based oil/gas platforms, main shafts of the offshore wind energy turbines, industrial chimneys, light houses and broadcasting towers. While being geometrically simple, this configuration creates a complex flow pattern in the near wake of the structure.

A relatively extensive literature exists on the vortex shedding around and on the vortex induced vibrations in straight (uniform) circular cylinders [1–5]. The literature on the flow and vortex shedding past tapered, as opposed to straight, circular cylinders is relatively scarce. This is partly due to the three dimensionality of the wake behind a tapered cylinder, which are rather difficult to be properly quantified and captured in experiments and in simulations. With a tapered cylinder the local Reynolds and Strouhal numbers, even under a uniform inflow, vary spanwisely. A range of flow-regimes such as steady wakes, laminar unsteady wakes and turbulent wakes may coexist around a tapered geometry. At higher Reynolds numbers the physics of the flow in the near wake become even more complicated. These make the numerical simulation of vortex shedding past tapered cylinders a very challenging task.

The literature on vortex shedding around tapered cylinders can be categorized into experimental and numerical studies, which are briefly reviewed below.

EXPERIMENTAL STUDIES

In his pioneer work, it has been addressed that vortex shedding past slender cones and tapered cylinders (taper ratios of 18 and 36) at Reynolds numbers ranging from 66 to 172 [6]. He concluded that velocity fluctuations in the cylinder wake are modulated. The modulated frequencies remain constant in regions along the cylinder span. Gaster and Hsiao called the region with a constant vortex shedding frequency a vortex cell [6, 7]. The region between two cells with different frequencies was referred to as transition region or as intersection region. Piccirillo reported that the spanwise length of a tapered circular cylinder can be divided to specified number of cells [8]. Each cell is characterized by its own vortex shedding frequency. It is worth noting that vortex shedding can also become cellular because of the cylinder end conditions, non-uniformity in the velocity profile or discontinuity in the cylinder diameter [9]. Papangelou discussed local diameters effects in wind tunnel tests on slightly tapered cylinders, at low Reynolds numbers (order of 100) [10]. He concluded that the cellular flow configuration is dependent on the Reynolds number at larger diameter and independent of the tip Reynolds number. He also reported that the frequency jump between adjacent cells is a function of flow speed, taper angle and kinematic viscosity. Piccirillo reported that, unlike straight cylinders, for tapered cylinders the vortex shedding pattern is unaffected by the cylinder end conditions [10].

Techet studied the flow in the wake of forced vibrating tapered circular cylinders in towing tank experiments. The Reynolds numbers ranged from 400 to 1500. They reported that no vortex cell was forming in the lock-in region and that a single frequency response dominated the entire spanwise length [11]. It was also concluded that within specific parametric ranges a hybrid mode is observed, consisting of a `2S' pattern along the part of the span with the larger diameter and a `2P' pattern along the part of the span with the smaller diameter.

Balasubramaniana investigated the relationship between the critical shear parameters in velocity and cellular vortex shedding at Reynolds number around 30,000. The results of the so called “aiding shear flow” on tapered circular cylinder showed cellular vortex shedding even for high shear parameters [13].Hsiao experimentally investigated cellular vortex shedding in tapered cylinders in a wind tunnel at sub-critical Reynolds number. Their results indicated the dependence of the Strouhal number (based on local diameter of the tapered cylinder) on the cylinder taper ratio [7]. Balasubramaniana experimentally studied vortex shedding in pivoted tapered circular cylinder subjected to uniform and shear velocity profiles. The Reynolds numbers ranged from 18,000 to 45,000 [14]. Their results demonstrated the sensitivity of lock-in range to the relative order of shear velocity gradient and axial taper of the cylinder.

More recently Zeinoddini et al. experimentally studied streamwise and crossflow vortex induced vibrations of single tapered cylinders [15]. Two tapered cylinders with different mean outer diameters (28 and 78 mm), mass ratios (6.1 and 2.27) and taper ratios (5 and 20) were considered. They have concluded that regardless of the taper or mass ratios, the lock-in range in tapered cylinders was wider than that in their equivalent uniform cylinder. Tapering had reportedly contradictory effects on the peak reduced cross-flow amplitude of the vibrations. For two tapered cylinders, it was reported that the mass ratio variation had more significant influence on the lock-in range and the peak reduced amplitudes of the cross- flow vibrations than the taper ratio.

Numerical Studies

It is noted that numerical simulation of the vortex shedding in the wake of a bluff body or flexible structures has only become feasible in the past two decades. This is because it typically requires massive computational efforts and advanced computation tools to solve the corresponding 3D transient Navier-Stocks equations. Vortex shedding around tapered cylinders in laminar flows was numerically simulated by Jespersen [16].Valles et al. numerically simulated vortex shedding in tapered circular cylinder with laminar flow at low Reynolds numbers (between 130 to 180, based on larger diameters of the cylinder) [17]. The simulation results show very good agreement with experimental data. Narsimhamurthy et al. simulated a tapered cylinder using an Immersed Boundary Method (IBM) [18]. Their predictions for the Strouhal number versus the local Reynolds number, however, did not accurately follow the experimental results. Parnaudeau et al. also carried out IBM direct numerical simulations of vortex shedding in tapered cylinders [19].

Xu and Zhu numerically simulated the crossflow and streamwise VIV of an elastically mounted cylinder [20]. They have compared the results with experimental data. Chen numerically simulated the 3D rigid circular cylinder within LES method of CFX5 [21]. Lift and Drag force coefficients and vortex patterns around the cylinder were investigated. Recently Ai numerically simulated unsteady flows around a 2D circular cylinder at high Reynolds number [22]. They have solved the 2D Unsteady Reynolds-Averaged Navier-Stokes (URANS) equations with a *k-ε* turbulence model.

In the current study the turbulent 3D vortex shedding phenomena on fixed tapered circular cylinders at subcritical Reynolds numbers is numerically investigated. Proper values for the sensitive parameters are selected by calibrating the model predictions against experimental data from other researchers. The calibrated model is further validated by comparing its predictions against different sets of small scale experimental vortex shedding data on tapered cylinder. The validated model is finally employed to study the detailed aspects of the vortex shedding phenomena in a tapered cylinder.

MODEL OUTLINES AND SENSITIVITY ASSESSMENT

Ansys-CFX12 computational fluid dynamics model is used to solve the 3D incompressible transient Navier-Stokes equations for simulating the flow and vortex shedding behind tapered cylinders at subcritical Reynolds numbers [23]. Overall dimensions of the computational domain, used in the sensitivity study, are shown in Figure 1(a). This model replicates wind tunnel experiments on linearly tapered cylinders (cones) carried out by Balasubramanian [13].Two uniform and tapered cylinders are simulated in different stages of the present study. The geometrical information of the two cylinders is included in Table 1.

A semi developed velocity profile, along the transverse direction of the domain, is introduced to the inlet boundary. A twelve-degree polynomial is used to define the flow velocity profile relative to the wall distance. The profile remains vertically (spanwisely) constant. A zero static pressure condition is introduced on the outlet boundary. It is noted that Balasubramaniana did not report data regarding the horizontal velocity profile in the wind tunnel. They only state that the horizontal velocity was uniform and equal to 11.35 m/s.

(a)

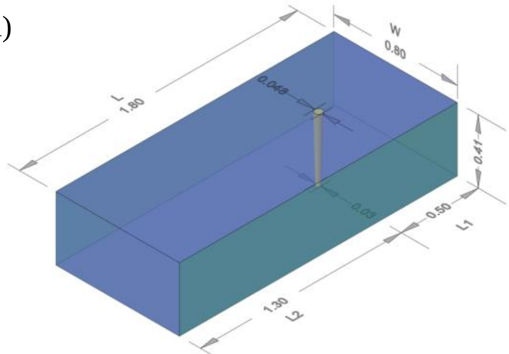

$$\frac{L_1}{D_{mean}} \approx 13, \frac{L_2}{D_{mean}} \approx 33.5, \frac{W}{D_{mean}} \approx 2$$

(b)

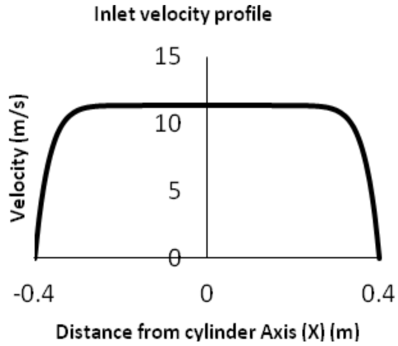

Fig. 1: *(a) Overall View the Computational Domain (Dimensions are in Meter and D is the Centrespan Diameter of the Tapered Cylinder) (b) Inlet Velocity profile (right) Considered in the Sensitivity Assessment and Validation of the Numerical Model.*

The velocity, inevitably, reduces to zero on the wind tunnel faces. The profile in Figure 1 which gives a velocity of 11.35 m/s in the best width of the fluid domain and drops to zero at two ends, is assumed to represent the horizontal velocity field throughout the experiment. Balasubramanian however, made measurements on the vertical velocity profile, which indicated on a constant wind speed of 11.35 m/s in the vertical direction [13]. This was because they considered two end plates on top and bottom of their test cylinder. For simulating the experiment velocity field in the experiment, a free slip wall condition is prescribed on the upper and lower side walls of the fluid domain.

The classical no-slip condition is included to the side walls of the computational domain and on outer surface of the cylinder. The above choices of wall boundaries are in agreement with other researchers like Kalro and Tezduyar LES studies and Balasubramaniana studies [24]. The inlet velocity profile in Figure 1 (b) is producing a horizontally uniform air flow velocity field of 11.35 m/s upstream of the cylinder. The computational time varies from 1 to 3 percent of the vortex shedding period [24].

The sensitivity analysis results indicate that the model behaviour, for Reynolds numbers ranging from 10,000 to 30,000, is very sensitive to i) the spatial grid resolution in the computational domain and ii) the type of turbulence model chosen for the analysis. Correct values for the sensitive parameters are decided through a course of model calibration, as presented in the next section.

MODEL CALIBRATION

Labbe and Wilson reported that for accurate estimation of 3D wakes instabilities, in a straight cylinder at Reynolds numbers higher than 300, simulating πD/2 to πD of the spanwise length is sufficient. A stationary three dimensional uniform circular cylinder at subcritical Reynolds number is used for calibrating the mesh resolution in the flow domain. The cylinder diameter and length are 0.05 and 0.157 meter, respectively. They correspond to those considered in the Dong and Karniadakis studies [25]. The inlet air flow velocity is 3m/s (Re=10,000).

Different computational mesh resolutions, varying in both planar and the spanwise directions of the domain, are considered. The computational mesh consists of two blocks. The first block encircles the cylinder and is formed by very fine, regular hexahedral elements. The unstructured second block is surrounding the first block and consists of mostly hexahedral elements, with a few prisms. Computational mesh characteristics for the five cases examined are summarized in Table 2. The table also gives the wall clock time for computing 1024 time steps on an Intel (R) Core™ i7 CPU 950 @ 3.07GHz personal computer (6GB RAM). LES-Smagorinsky turbulent model is considered with all five models.

Table 1: *The Geometrical Information of the Two Cylinders Simulated in Current Study.*

Cylinder	$D_{min\ (cm)}$	$D_{max\ (cm)}$	Length	Re	Remark
Tapered	3.016	4.76	41.28	10,000	Replicates wind tunnel experiments by Balasubramanian et al. [13].
Uniform	D		πD	29,000	Replicates Dong and Karniadakis [25] DNS Studies.

Table 2: *Details of the Five Computational Mesh Resolutions.*

Mesh number	First inflation layer thickness (m)	Number of span wise divisions	y+	z+	Number of elements	Number of nodes	Wall clock time for 1024 time steps (hour)	
							Parallel Runs (8 partitions)	Serial Runs
1	1.5×10^{-5}	45	0.30	1.65	832,095	858,176	11	-
2	1.5×10^{-5}	16	0.32	1.75	295,184	316,472	-	9
3	5×10^{-5}	45	1	1.64	500,220	579,064	-	16
4	5×10^{-5}	32	0.98	1.68	355,712	372,372	-	12
5	5×10^{-5}	16	1.1	1.75	177,856	191,828	-	6

Check point results from each simulation are presented in Table 3. They include the Strouhal number plus the lift and drag coefficients. Corresponding direct numerical simulation (DNS) results from Dong and Karniadakis and some experimental data are also provided for comparison [25]. Table 3 shows that the number of spanwise divisions has a remarkable effect on the models' predictions. A low number of subdivisions

(Mesh 2 and Mesh 4 with N=16) provides the poorest predictions, as compared to the experimental results and those from the DNS-B3 model from Dong and Karniadakis [25].Mesh 4 with N=32 provides the best predictions for the Strouhal number and the lift and drag coefficients. Mesh 4 might seems relatively course but extra refinements in the spanwise subdivisions (Mesh 1 and Mesh 3 with N=45) is counterproductive. It seems that for an accurate simulation, there might be a certain proportion between the length and diameter of the cylinder and the number of spanwise divisions. Here Mesh 4 with N=32 provides the best predictions but selection of an optimum number of spanwise divisions needs some more investigation which can be included in the future works.

As it can be seen in Table 3, utilizing a very fine mesh in the planar direction costs longer computations without much improvement in accuracy. It should be noted that in the selection of the most optimum grid refinement one should consider the computational cost. Table 3 indicates that the efficiency of the parallel run relative to a serial run, assuming that the problem is stationary, is around 30%, which does not seem very high. This is partly because the performance determination is not sometimes straightforward due to the fact that only part of the solver run is actually performed in parallel. The reading and distributing of the solver input file data, and the collecting and writing of results file data are highly I/O dependent and not parallelized. These stages, therefore, depend on high disk speeds and fast network communication for fast operation (ANSYS, Inc. April). Time stepping and convergence also play a role in the computation performance. It is noted that identical time stepping and convergence criteria are considered for the parallel and serial runs. Mesh 4 seems to provide reasonable agreement with the experimental results and those from the DNS-B3 model from Dong and Karniadakis, while demanding relatively low computational efforts. Figure 2 provides comparisons between the predictions from Mesh 4 and the DNS results from Dong and Karniadakis [25].The time histories of the lift and drag coefficients from the two studies are presented in the Figure 2. In general, Figure 2 presents a reasonable agreement between the simulation results from the current study and the DNS results Figure 2 the C_L (lift coefficient) amplitude from the current study is somewhat larger than that from Dong and Karniadakis (around 11% differences in the C_L RMS)[25]. This can be attributed to the fact that the current study employs a LES turbulence modelling approach while the Dong and Karniadakis results are based on a direct numerical simulation (DNS). It is worth noting that the model used in the current study requires a considerably lower computation time as compared to the DNS simulations which took advantage of parallel performance of a Compaq Alpha cluster with 1536 processors (Table 3).

Numerical results presented in Table 3 are obtained by considering a Large Eddy Simulation (LES) [26] turbulence model with Smagorinsky subgrid scale viscosity. Table 3 indicates that the LES-Smogorinsky model (e.g. Mesh No. 4) is able to provide predictions reasonably close to the experimental measurements. This falls in line with findings from other researchers. For example, Murakami and Rodi compared the capability of the LES model with other well known models like K-ε and Algebraic Stress models when simulating the flow around bluff bodies [27, 28]. They concluded that the LES model provides reliable and accurate simulations of the flow characteristics.

Effects of three different LES subgrid-scale models, namely the Wall-Adapted Local Eddy-Viscosity model or WALE model Nicoud and Ducros, the Smagorinsky model and the Dynamic Smagorinsky-Lilly model, on the simulation results (of uniform cylinder described in this Section) are investigated. Check point results from each simulation, such as the Strouhal number and lift and drag coefficients, are presented in Table 4 [27–31]. As it can be noticed the Smagorinsky model provides better predictions as compared to the Direct Numerical Simulation (DNS) results by Dong and Karniadakis and experimental data (Table 3). As a result the LES turbulence model with Smagorinsky subgrid scale viscosity is used for the rest of simulations reported.

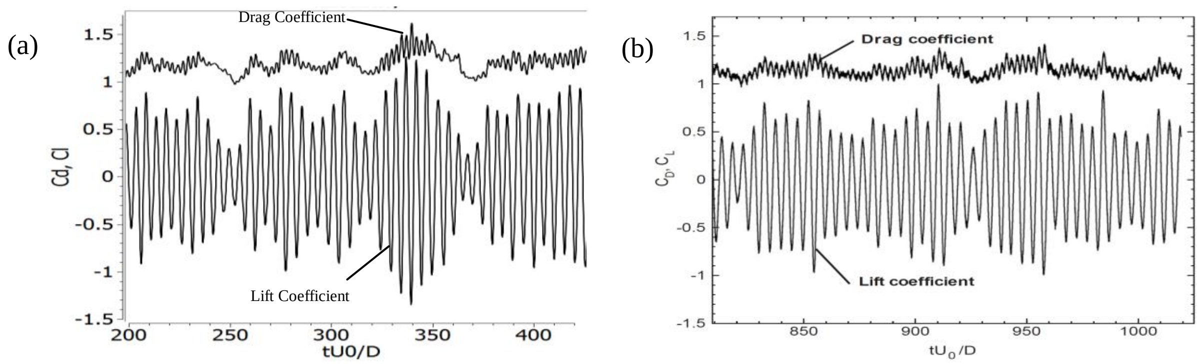

Fig. 2: *Time Series of the Lift and Drag Coefficients for the Flow past a Stationary Uniform Cylinder from (a) Mesh 4 (see Table 2) in the Current Study (b) Direct Numerical Simulation by Dong and Karniadakis. (T is time in second, U_0 is the Upstream Flow Velocity in m/s and D is the Cylinder Diameter in Meter, C_l is the Lift and C_d is the Drag Coefficient).*

Table 3: *Results Check Points for the Computation Mesh Resolution, Including Lift and Drag Coefficients and Strouhal Number.*

Description	RMS lift coefficient	Mean drag coefficient	Strouhal number	Wall clock time for 1024 time steps (hour)
Mesh 1 (current study)	0.589	1.23	0.191	11 hours of parallel runs (8 partitions)
Mesh 2 (current study)	0.798	1.33	0.202	9 hours of serial run
Mesh 3 (current study)	0.56	1.21	0.197	16 hours of serial run
Mesh 4 (current study)	0.502	1.16	0.198	12 hours of serial run
Mesh 5 (current study)	0.78	1.29	0.208	6 hours of serial run
DNS-A1[25]	0.538	1.155	0.195	20,000 to 250,000 hours
DNS-A2 [25]	0.565	1.11	0.209	
DNS-A3 [25]	0.574	1.128	0.205	
DNS-B1 [25]	0.547	1.208	0.200	
DNS-B2 [25]	0.497	1.12	0.205	
DNS-B3 [25]	0.448	1.143	0.203	
Wieselsbebrger [37]	-	1.143	-	Experiment
Bishop and Hassan [38]	0.463	-	0.201	Experiment
Moeller and Leehey [39]	0.532	-	-	Experiment
West and Apelt [40]	0.461	1.186	-	Experiment
Norberg [41]	0.394	-	0.202	Experiment

Table 4: *Effects of Three Different LES Subgrid-Scale Models on the Results Check Points.*

Computational mesh	Subgrid-scale model	Strouhal number	Mean drag coefficient	Lift coefficient (RMS)
Numerical model: Mesh4	Smagorinsky	0.198	1.16	0.502
	Dynamic Smagorinsky-Lilly model	0.194	1.18	0.532
	WALE model	0.189	1.36	0.788

Calibration results (Table 3 and Figure 2) showed that Mesh 4 provides reasonable predictions for Strouhal number, drag and lift coefficients and temporal variations of the two coefficients, as compared to the Dong and Karniadakis and the experimental results [25]. The model also requires low computational efforts. These, however, cannot guarantee that the model will function correctly with other geometries or other flow conditions. It is, therefore, necessary to further validate the model against different experiments and to verify if it represents the physics of the problem properly. The model verification will be discussed in Section 4 and its predictions for the physics of the vortex shedding behind a tapered cylinder will be provided in Section 5.

MODEL VALIDATION

The experimental results from Balasubramaniana et al. are used for the validation of the numerical model employed in the current study. They carried out wind tunnel tests on a stationary tapered solid aluminium cylinder under uniform and linear shear flows [13]. Data on the cylinder geometry and the inlet velocity are provided in Table 5. The work of Balasubramanian includes vortex shedding behind one tapered cylinder under both uniform and shear flow regimes. Only one experimental output for the uniform flow is presented in the paper. Their result for uniform flow (Figure 3(b)) is used for the verification of our model. To provide further validations of the model we also compare our results with those from a different experimental work [7].Mesh resolution No. 4 (Table 2) is used for the simulations reported in this section. 108 equally spaced divisions are considered in the spanwise direction. The LES turbulence model with a Smagorinsky subgrid-scale scheme is used. The boundary conditions on the cylinder surfaces and on the fluid domain are the same as described in Section 2.

Fourier representations of the horizontal velocity in the wake of the stationary tapered cylinder, from the simulations (current study) and the experiments are provided in Figure 3 [13]. The monitoring points have a coordinate of 10.16 cm in the streamwise direction and 3.3cm in cross stream direction from the cylinder axis. The dominant vortex shedding frequencies at different spanwise elevations from the current simulation (Figure 3(a)) appear to be in reasonable agreements with the corresponding experimental results (Figure 3(b)). As it can be noticed, the dominant vortex shedding frequency experiences, spanwise, changes of 50 to 76 Hz.

Spanwise spectra from the experiments (Figure 3(b)) are comparatively smoother and broader than those obtained in the current simulations. This is most likely because the total measurement time in the experiment is significantly higher than the simulation duration. Long time series are likely to produce smooth and broad spectra. In general, the calibration and validation results presented in Sections 3 and 4 reveal that the current computational model allows for an acceptable simulation of the vortex shedding past a tapered cylinder.

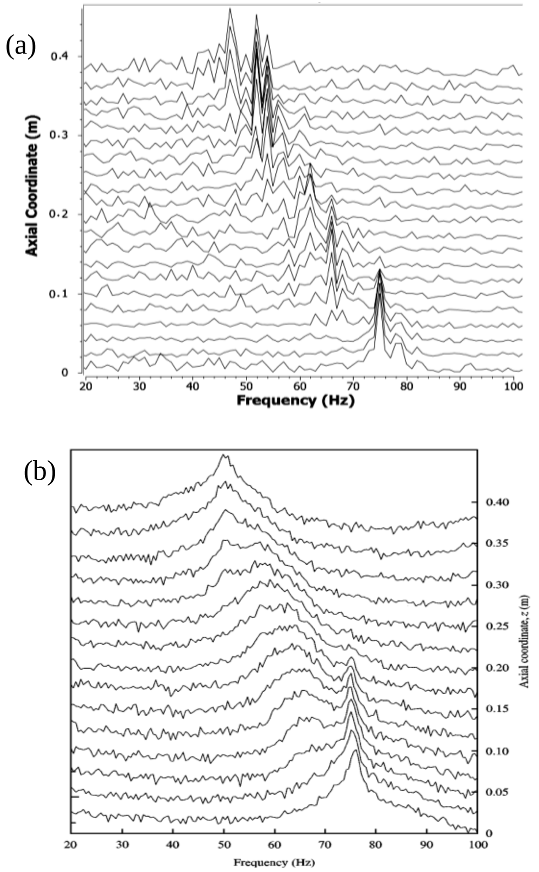

Fig.3: *Spanwise Spectral Analysis of the Velocity Time Series in the Wake of the Stationary Tapered Cylinder from (a) The Current Study and (b) Experiments by Balasubramanian et al.[13].*

Table 5: *Geometries of the Tapered Cylinder and the Upstream Velocity used in the Wind Tunnel Tests by [13] and in The Model Verification (current study).*

Inlet velocity (m/s)	Smaller end diameter (cm)	Larger end diameter (cm)	Re (based on D_{mean})	Length of the tapered cylinder (cm)	Taper ratio
11.35	3.016	4.76	29419	41.28	23.7

RESULTS AND DISCUSSIONS

The computational model explained in previous sections is used to explore vortex shedding characteristics past linearly tapered cylinders in subcritical Reynolds numbers. The flow velocity and cylinder dimensions are given in Table 5. Different phenomena such as variation of the shedding frequency along the cylinder span or cellular vortex shedding, vortex dislocations or vortex splitting, oblique vortex shedding, streamwise and spanwise vortices and the variation of the vorticity patterns along the tapered cylinder are well demonstrated by the numerical model. Time histories of the lift and drag force coefficients of the tapered cylinder are also provided. This section summarizes and discusses some of the results and observations.

Vortex Splitting

By making use of pseudo-flow visualization technique, which was developed by Wat, the vortex splitting or dislocations can be identified [32]. Numerical results for the time history of the pressure and velocity at arbitrary monitor points in the wake of the stationary tapered cylinder are presented in Figure 4. The monitoring points have a coordinate of 10.16 cm in streamwise direction and 3.3cm in cross stream direction from the cylinder axis.

In addition, timeframes of the pressure and velocity contours are provided in the left sides of Figure 4. The red colours represent the peaks (local maxima) and the blue colours denote the valleys (local minima). The pressure or velocity peaks demonstrate the passageways of the vortices [7]. Therefore, red areas in the left figures show the spanwise spreading of the vortex lines in the wake of the tapered cylinder. A kink in the vortex line (see Figure 4) indicates the onset of a vortex splitting (or vortex dislocation). As it can be seen, both the velocity and pressure contours depict very similar vortex spreading patterns in identical time intervals.

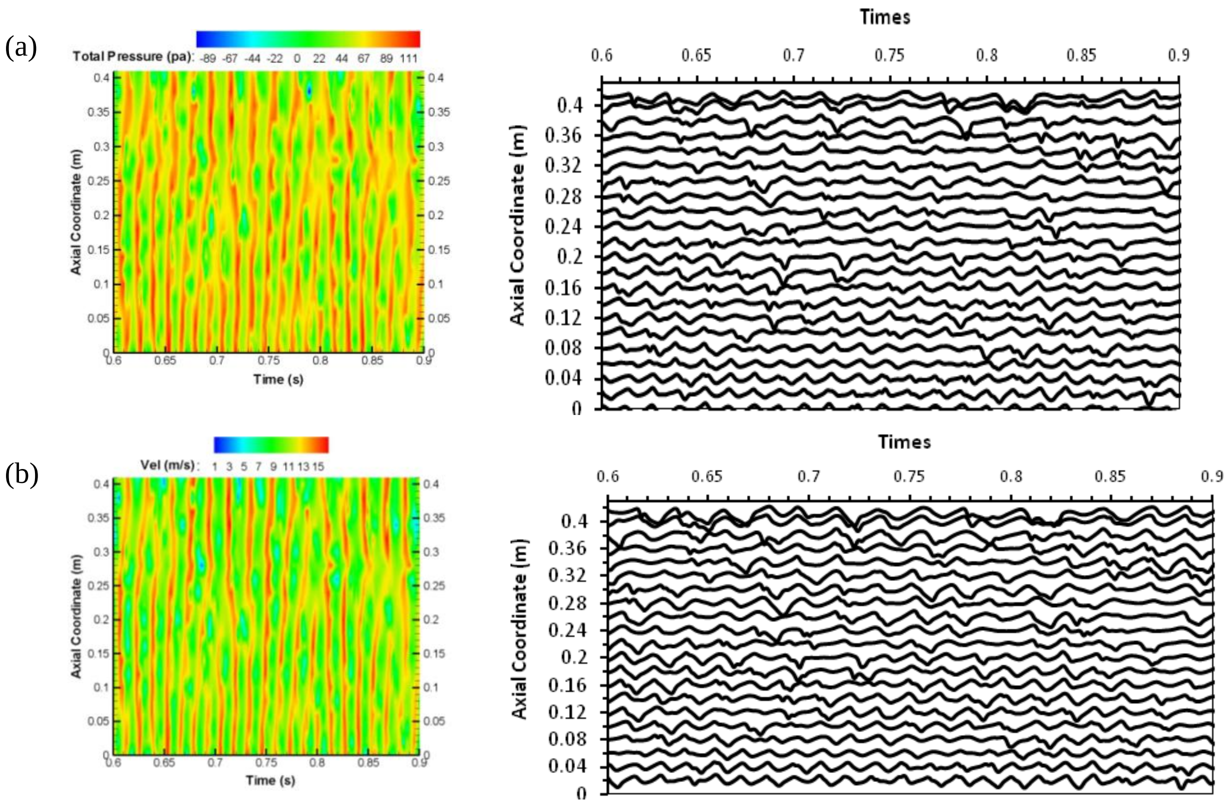

Fig. 4: *Pseudo-Flow Visualization. (a) Pressure Fluctuation (b) Velocity Fluctuation. Time histories of the Pressure/Velocity Fluctuation (right), Contour Lines of the Pressure/Velocity (left).*

Cellular Vortex Shedding

In order to specify the number of spanwise vortex cells, the numerical predictions for the Strouhal numbers along the cylinder axis are extracted and presented in Figure 5. The results are for a cylinder with a taper ratio of 23.7 in a Reynolds number of around 29,000. The geometrical properties remain the same as those given in Table 5. A spanwise region with an unvarying Strouhal number represents a vortex cell. Each zone indicates a discrete shedding cell, with its own constant shedding frequency. For defining the Strouhal numbers we follow the approach considered by Hsiao [7]. They used the mean diameter of the tapered cylinder for this calculation. We follow the suit to provide a basis for the comparison between their results and those from the current study. The Strouhal numbers might also be defined based on local diameter at *z/L*, like St (*z*) =*f D* (*z/L*)*/U*. In that case the graphs provided in Figure 5 may become much flatter. From Figure 5(a), five distinctive shedding cells, along the tapered cylinder axis, can be identified. For the sake of comparison the Strouhal numbers in experiments carried out by Hsiao [7] are also presented in Figure 5. The centre span diameter and the length of the tapered cylinder employed in the test were similar to those used in the current numerical model but the taper ratio was 24.4. The Reynolds number was 14,000. Figure 5 shows that the experimental Strouhal numbers at two ends slightly differ from those of the numerical model. The number of vortex cells in the experiment is four. The lengths of the associated vortex cells in the experiment and in the numerical results are not the same. These differences are attributed to the fact that the Reynolds number and the taper ratio in the numerical model (current study) and the test are different [7]. Time histories of the lift and drag coefficients of the tapered cylinder are shown in Figure 6. The RMS of the lift coefficient and the mean drag coefficient is 0.15 and 0.98, respectively.

Oblique Vortex Shedding

Oblique, versus parallel, shedding is a distinctive feature of the vortex dynamics in the wake of tapered cylinder. This phenomenon is captured during vortex shedding experiments in a uniform stream past tapered cylinders and in a shear flow past straight cylinders. In a uniform stream, end effects can also trigger oblique shedding behind uniform circular cylinders.

(a)

(b)

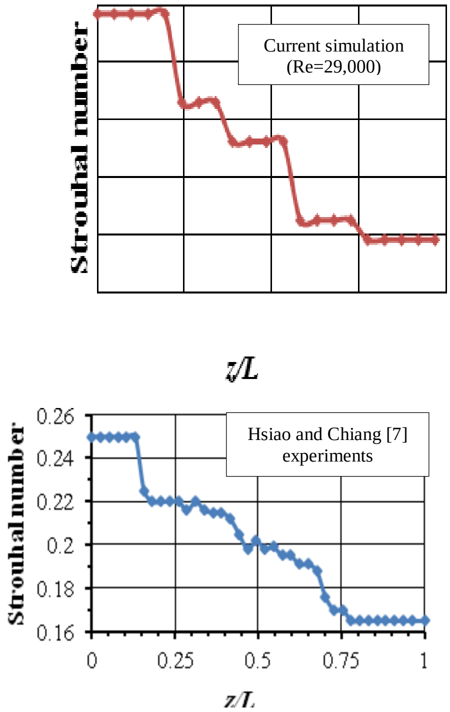

***Fig. 5:** Numerical Predictions (current study) and Experimental Data [7] for the Strouhal Number Variation along a Tapered Cylinder Axis (z).*

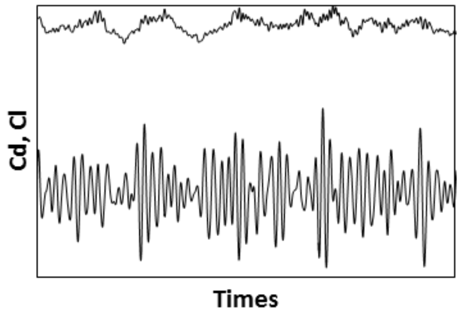

***Fig. 6:** Time Histories of the Lift and Drag Coefficients of the Tapered Cylinder.*

For tapered cylinders, the oblique vortex shedding phenomenon is primarily caused by the geometrical inhomogeneity along the span. The obliqueness angle between the shed vortices and the cylinder axis was reported to vary from 5^o to 25^o, before vortex splitting occurs. During each split, the vortex lines far away continue to steepen up to 50^o [17].

Figure 7 depicts results from the current study for the instantaneous vorticity contours in the wake of a stationary tapered cylinder. The Reynolds number is 29,000. The blue areas in Figure 7 show negative or clockwise vorticities and the red areas denote positive or anti-clockwise vorticities. Figure 7(b) shows the vorticity contours in a spanwise-streamwise plane passing the cylinder axis. Figure 7(a) gives the vorticity contours in three planar sections along the cylinder span. The planar sections are located close to the two ends and in the mid span of the cylinder. From Figure 7(a), evolution of oblique vortex shedding behind the tapered cylinder together with the vortex dislocation can be appreciated. Patterns of vortex shedding, with a strong obliqueness, and their splitting are clearly demonstrated in Figure 7(b). Kinks in vortex lines, which indicate on onsets of vortex splitting, can be noticed in Figure 7(a) and Figure 7(b).

(a)

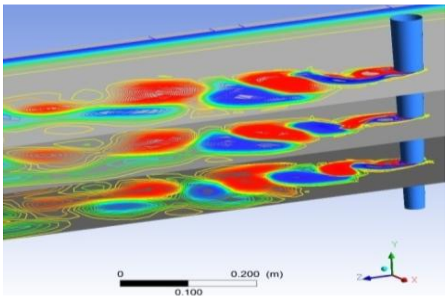

(b)

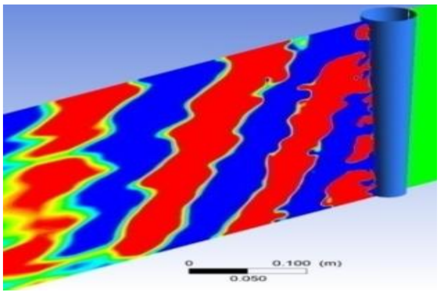

Fig. 7: *Numerical Results (current study) for the Distribution of Instantaneous Vorticity Contours in the Wake of the Stationary Tapered Cylinder. Blue Areas Show Negative and Red Areas Present Positive Vorticities.*

Longitudinal Vortices

In the dye visualization of vortex shedding patterns past uniform cylinders at Reynolds number greater than 140, Gerrard noticed the existence of 3D structures in the form of "dye fingers" along the cylinder span[33]. Wu et al. related these finger type patterns to the existence of longitudinal vortices inclined relative to the streamwise direction [34]. These so called dye fingers were named by Techet as streamwise vortices [12]. They are also known as longitudinal vortices or ribs. Wu et al. reported that these longitudinal vortices wander along the span of the cylinder. Measurements on the velocity fields in the wake of cylinders by Hayakawa and Hussain substantiated formation of longitudinal vortices in the wake of straight cylinders [34–41]. They called these three-dimensional characters of the wake as ribs wrapping around rolls or ribs in the braid.

The model used in the current study also successfully captured the longitudinal vortices or ribs at the near wake of the tapered cylinder. The geometrical properties of the simulated tapered cylinder remain the same as those given in Table 5 and the Reynolds number is around 29,000. Figures 8(a), (b) give the instantaneous isosurfaces of the total pressure and the isocontours of the spanwise vorticities, respectively. They clearly demonstrate the presence and evolution of longitudinal vortices (or the so called fingers) along the cylinder span. Figures 8(c) to Figure 8(f) illustrate the evolution of the longitudinal vortices in the wake of the tapered cylinder. These figures depict the streamwise vorticity contours on a vertical plane in the near wake of the tapered cylinder. The presence of three-dimensionality in the wake region can be inferred from these figures. It can be seen that the streamwise vortices are almost paired and their intensity is relatively higher at the mid span of the cylinder. Furthermore, the intensity of the streamwise vorticity is much higher than the corresponding spanwise vorticity. These types of three dimensionality effects are an important feature of the vortex dynamics in tapered cylinder wakes. The complex three dimensional natures of the wakes behind a tapered cylinder can be understood from Figure 9. The figure depicts the instantaneous streamwise vorticities in the wake of the tapered cylinder. Figure 9 indicates that longitudinal vortices do exist in the far downstream of the cylinder. It is noted that the axial diffusion of streamwise vortices, caused by the longitudinal vorticity, may have an important effect on the response of a flexible tapered cylindrical structure in uniform and non-uniform flow field.

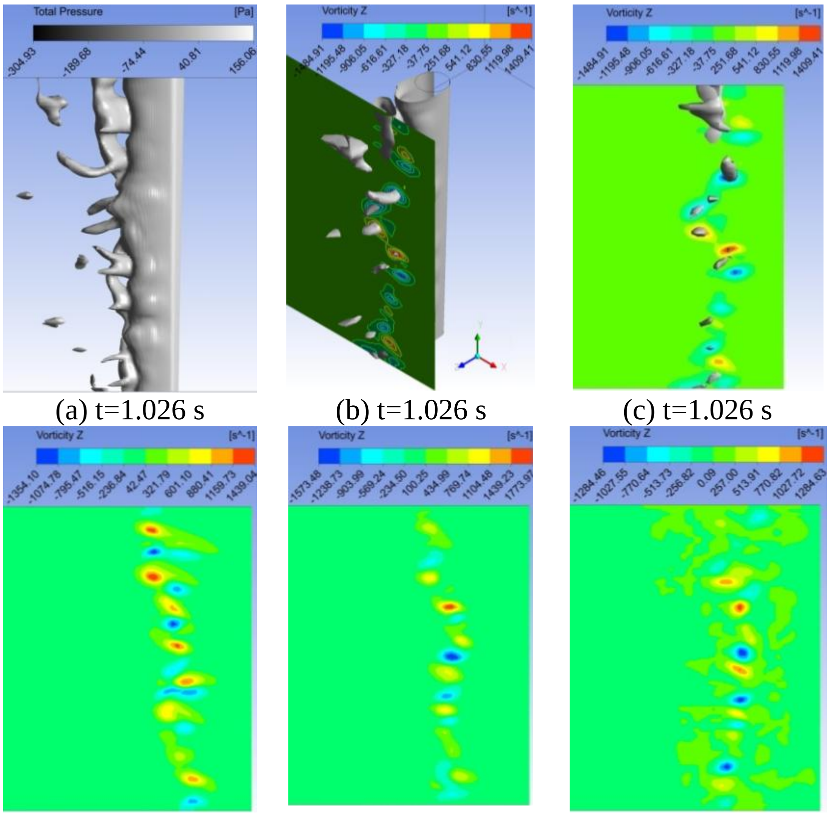

(a) t=1.026 s (b) t=1.026 s (c) t=1.026 s

(d) t=1.029 s (e) t=1.032 s (f) t=1.035 s

Fig. 8: *Instantaneous Streamwise Vortices. (a) Finger Shape Patterns at the Near Wake of the Tapered Cylinder. (b–f) Evolution of the Streamwise Vortices Over Time.*

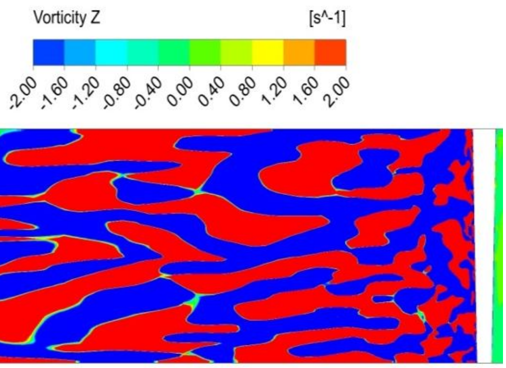

Fig. 9: *The Instantaneous Streamwise Vorticity in the Wake of the Tapered Cylinder.*

CONCLUSIONS

Turbulent 3D vortex shedding phenomena past a tapered stationary cylinder under a uniform flow at subcritical Reynolds numbers is studied. A numerical approach based on the solution of 3D transient Navier-Stokes equations is considered. The sensitivity analysis results indicate that the model behaviour is very sensitive to i) the grid resolution in the computational domain and ii) the turbulence model. Different turbulence models and mesh resolutions are tested in the sensitivity analysis. The computational mesh of the numerical model is calibrated with others DNS and experimental results. The LES turbulence model with a Smagorinsky subgrid-scale scheme is found to provide a reasonable estimate for the dominant vortex shedding frequency in the wake of a tapered cylinder as compared to experimental data. The model is also validated against separate sets of experimental data. Reasonable quantitative agreements are obtained between the model predictions, for the vortex shedding past a tapered circular cylinder, and the experimental results from other researchers.

The numerical model is then used to investigate vortex shedding characteristics past tapered cylinders. Key physical characteristics such as vortex dislocations and splitting, cellular vortex shedding, oblique vortex shedding and the variation of the vorticity patterns along the tapered cylinder are successfully simulated and captured. The lift and drag force coefficients of the tapered cylinder are also calculated.

REFERENCES

1. Parkinson G.V., Mathematical models of flow-induced vibrations of bluff bodies In Flow Induced Structural Vibrations (ed. E. Naudascher) *Springer*, Berlin, 1974.
2. Bearman P.W., Vortex shedding from oscillating bluff bodies. *Annual Review of Fluid Mechanics*, 1984; 16:195–222p.
3. Williamson C.H.K., Govardhan R., Vortex-induced vibrations. *Annual Review of Fluid Mechanics*, 2004; 36: 413–455p.
4. Williamson C.H.K., Govardhan R., A brief review of recent results in vortex-induced vibrations, *Journal of Wind Engineering a nd Industrial Aerodynamics*, 2008; 96: 713 –735p.
5. Gabbai R.D., Benaroya H., An overview of modeling and experiments of vortex-induced vibration of circular cylinders. *Journal of Sound and Vibration*, 2005; 282–575p.
6. Gaster M., Vortex shedding from slender cones at low Reynolds numbers. *J. Fluid Mech.*, 1969; 38: 565–576p.
7. Hsiao F.B., Chiang C.H., Experimental study of cellular shedding vortices behind a tapered circular cylinder. *Experimental Thermal and Fluid Science*, 1998; 17: 179–188p.
8. Piccirillo P.S., Van Atta C.W., An experimental study of vortex shedding behind linearly tapered cylinders at low Reynolds number. J. Fluid Mech, 1993; 246: 163–195p.
9. Hsiao F.B., Pan J.Y., Chiang C.H., The study of vortex shedding frequencies behind tapered circular cylinders. *Symposium on Flow-Induced Vibration and Noise, ASME*, 1992; 6: 103±112p.
10. Papangelou A.,Vortex shedding from slender cones at low Reynolds numbers. *J. Fluid Mech.*, 1992; 242: 299–321p.
11. Techet A.H., Hover F.S., Triantafyllou M.S., Vertical patterns behind a tapered cylinder oscillating transversely to a uniform flow. *J. Fluid Mech*, 1998; 363: 79–96p.
12. Techet A.H., Vortical patterns behind a tapered cylinder. M.Sc, MIT.1998.
13. Balasubramaniana S., Haan F.L., Szewczyk A.A., Skop R.A., On the existence of critical shear parameter for cellular vortex shedding from cylinders in nonuniform flow. *Journal of Fluids and Structures*, 1998; 12: 3–15p.
14. Balasubramaniana S., Haan F.L., An experimental investigation of the vortex-excited vibrations of pivoted tapered circular cylinders in uniform and shear flow. Journal of Wind Engineering and Industrial Aerodynamics, 2001; 89: 757–784p.
15. Zeinoddini M., Tamimi V., Seif M.S., Stream-wise and cross-flow vortex induced vibrations of single tapered circular cylinders: An experimental study. *Journal of Applied Ocean Research*, 2013; 42: 124–135p.
16. Jespersen D.C., Levit C., Numerical simulation of flow past a tapered cylinder, *NAS Technical Report RNR*-90-021.1990.
17. Vall`es B., Andersson H.I., Jenssen C.B., Oblique vortex shedding behind tapered cylinders. *J. Fluids Struct*. 2002; 16: 453–463p.
18. Narasimhamurthy V.D., Schwertfirmk F., Andersson H.I. et al., Simulation of unsteady flow past tapered circular cylinders using an Immersed Boundary Method. Norwegian University of Science and Technology (NTNU), *European Conference on Computational Fluid Dynamics ECCOMAS CFD*.2006.
19. Parnaudeau P., Heitz D., Lamballais E., Silvestrini J.H., Direct numerical simulations of vortex shedding behind cylinders with spanwise linear nonuniformity.*Proc.TSFP4*, 2005; 111-116p.
20. Xu J.L., Zhu R.Q., Numerical simulation of VIV for an elastic cylinder mounted on the spring supports with low

mass-ratio. *Journal of Marine Science and Application*, 2009; 3: 237–245p.

21. Chen H.L., Dai S.S., Li J. et al., Three-dimensional numerical simulation of the flow past a circular cylinder based on LES method. *Journal of Marine Science and Application*, 2009; 2: 110–116p.
22. Ai Y., Feng D., Ye H., Unsteady numerical simulation of flow around 2-D circular cylinder for high Reynolds numbers. *Journal of Marine Science and Application*, 2013; 2: 180–184p.
23. ANSYS CFX Reference Guide. Release 12.0. ANSYS, Inc. April 2009. Southpointe. 275 Technology Drive. ANSYS, Inc. certified to ISO. 9001:2008.
24. Kalro V., Tezduyar T., Parallel 3D computation of unsteady flows around circular cylinders. Parallel Computing, 1997; 23: 1235–1248p.
25. Dong S., Karniadakis G.E., DNS of flow past a stationary and oscillating cylinder at Re 10000. Journal of Fluids and Structures, 2005; 20: 519–531p.
26. Pope S.B., Turbulent Flows. Cambridge University Press.2000.
27. Murakami S., Comparison of various turbulence models applied to a bluff body. *Journal of Wind Engineering and Industrial Aerodynamics*, 1993; 46: 21–36p.
28. Rodi W., On the simulation of turbulent flow past bluff bodies. *Journal of Wind Engineering and Industrial Aerodynamics*, 1993; 46:3–19p.
29. Nicoud, F., Ducros, F., Subgrid-scale stress modelling based on the square of the velocity gradient tensor. *Flow, Turbulence and Combustion*, 1999; 62: 183–200p.
30. Smagorinsky J., General circulation experiments with the primitive equations. *Month. Weath. Rev*.1963; 93: 99–165p.
31. Lilly D.K., A proposed modification of the Germano subgrid-scale closure method. *Phys. Fluids, 1992;* 3: 633–635p.
32. Wat J.K., The unsteady and radiation behaviour of a jet. *PhD. Thesis*, Department of Aerospace Engineering, University of Southern California, Los Angeles, CA.1998.
33. Gerrard J.H., The wakes of cylindrical bluff bodies at low Reynolds number. *Philos. Trans. R. Soc. London*, 1978; 288: 351–378p.
34. Wu J., Sheridan J., Welsh M.C. et al., Three-dimensional vortex structures in a cylinder wake. *J. Fluid Mech*, 1996; 312: 201–222p.
35. Wu J., Sheridan J., Welsh M.C. et al., Longitudinal vortex structures in a cylinder wake. *Physics of Fluids*, 1994; 6(9): 28885–2885p.
36. Hayakawa M., Hussain F., Three-dimensionality of organized structures in a plane turbulent wake. *J. Fluid Mech*., 1989; 206: 375–404p.
37. Wieselsberger C., Neuere Feststellungen uber die Gesetze des Flussigkeits und Luftwiderstands. Physikalische Zeitschrift, 1921; 22: 321–328p.
38. Bishop R.E.D. Hassan A.Y., The lift and drag forces on a circular cylinder in a flowing fluid. Proceedings of Royal Society London, 1964; A 277: 32–50p.
39. Moeller M.J., Leehey P., Unsteady forces on a cylinder in cross flow at subcritical Reynolds numbers. In: Paidoussis, M.P.1984.
40. West G.S., Apelt C.J., Measurements of fluctuating pressures and forces on a circular cylinder in the Reynolds number range. *Journal of Fluids and Structures, 1993;* 7: 227–244p.
41. Norberg C., Fluctuating lift on a circular cylinder: review and new measurements. Journal of Fluids and Structures, 2003; 17: 57–96p.

NOMENCLATURE

D	Diameter of the uniform cylinder	L	Cylinder length
D_{mean}	Mean diameter of the tapered cylinder	n	Kinematic viscosity
D_{Max}	Larger diameter of the tapered cylinder	F_L	Total lift force
D_{Min}	Smaller diameter of the cylinder	F_d	Total drag force
V	Current velocity	f_s	Vortex shedding frequency in the wake
C_l	$Lift\ \ coefficient = \frac{2\ \ F_L}{(\rho V^2 D_{mean} L)}$	C_d	$Drag\ \ coefficient = \frac{2\ \ F_d}{(\rho V^2 D_{mean} L)}$
R_T	$Taper\ \ ratio = \frac{L}{D_{\max} - D_{\min}}$	S_t	$Strouhal\ \ number = \frac{f_s}{D_{mean}\ \ V}$
Re	$\mathrm{Re}ynolds\ \ number = \frac{V\ \ D_{mean}}{\upsilon}$		